

LETTER TO THE EDITOR

A bright $z=5.2$ lensed submillimeter galaxy in the field of Abell 773 HLSJ091828.6+514223

F. Combes¹, M. Rex², T. D. Rawle², E. Egami², F. Boone³, I. Smail⁴, J. Richard⁵, R.J. Ivison⁶, M. Gurwell⁷, C.M. Casey⁸, A. Omont⁹, A. Berciano Alba¹⁰, M. Dessauges-Zavadsky¹¹, A.C. Edge⁴, G.G. Fazio⁷, J-P. Kneib¹², N. Okabe¹³, R. Pelló³, P. G. Pérez-González¹⁴, D. Schaerer^{11,3}, G.P. Smith¹⁵, A.M. Swinbank⁴, and P. van der Werf¹⁶

(Affiliations can be found after the references)

Received December 28, 2011 / Accepted January 16, 2012

ABSTRACT

During our *Herschel* Lensing Survey (HLS) of massive galaxy clusters, we have discovered an exceptionally bright source behind the $z=0.22$ cluster Abell 773, which appears to be a strongly lensed submillimeter galaxy (SMG) at $z=5.2429$. This source is unusual compared to most other lensed sources discovered by *Herschel* so far, because of its higher submm flux (~ 200 mJy at $500\mu\text{m}$) and its high redshift. The dominant lens is a foreground $z=0.63$ galaxy, not the cluster itself. The source has a far-infrared (FIR) luminosity of $L_{\text{FIR}} = 1.1 \cdot 10^{14} / \mu L_{\odot}$, where μ is the magnification factor, likely ~ 11 . We report here the redshift identification through CO lines with the IRAM-30m, and the analysis of the gas excitation, based on CO(7-6), CO(6-5), CO(5-4) detected at IRAM and the CO(2-1) at the EVLA. All lines decompose into a wide and strong red component, and a narrower and weaker blue component, 540 km s^{-1} apart. Assuming the ultraluminous galaxy (ULIRG) CO-to- H_2 conversion ratio, the H_2 mass is $5.8 \cdot 10^{11} / \mu M_{\odot}$, of which one third is in a cool component. From the $\text{C I}(\text{}^3\text{P}_2 - \text{}^3\text{P}_1)$ line we derive a $\text{C I}/\text{H}_2$ number abundance of $6 \cdot 10^{-5}$ similar to that in other ULIRGs. The $\text{H}_2\text{O}_p(2,0,2-1,1,1)$ line is strong only in the red velocity component, with an intensity ratio $I(\text{H}_2\text{O})/I(\text{CO}) \sim 0.5$, suggesting a strong local FIR radiation field, possibly from an active nucleus (AGN) component. We detect the $[\text{NII}]205\mu\text{m}$ line for the first time at high- z . It shows comparable blue and red components, with a strikingly broad blue one, suggesting strong ionized gas flows.

Key words. Galaxies: evolution — Galaxies: high-redshift — Galaxies: ISM — Infrared: galaxies — Submillimeter: galaxies — Galaxies: Individual: HLSJ091828.6+514223

1. Introduction

At high redshift, $z \sim 1-3$, dusty luminous infrared galaxies are thought to dominate the history of cosmic star formation (Dole et al. 2006; Wardlow et al. 2011). At these epochs, star formation was occurring mainly in massive galaxies, a tendency dubbed downsizing in galaxy formation scenarios (e.g. Cowie et al. 1996; Heavens et al. 2004; Pérez-González et al. 2008; Magnelli et al. 2009, 2011). These massive starbursts might correspond to the formation phase of the luminous ellipticals seen in high-density regions today (Genzel et al. 2003; Swinbank et al. 2006). They are therefore essential for understanding the main processes of galaxy formation and evolution. In particular, atomic and molecular lines are crucial clues in these systems for tackling star formation and AGN (Active Galaxy Nucleus) activities (Riechers et al. 2010, 2011; Danielson et al. 2011).

Owing to the negative K-correction, the number of submillimeter galaxies (SMGs) does not need to peak at $z \sim 1-3$, indeed, if they exist, they should be as easy to detect at $z=8$ as they are at $z=1-3$. Their observed dearth is probably due to evolution of gas fraction and halo mass (Lacey et al. 2010; Hickox et al. 2011). To be able to make a census of $z \sim 5$ SMG and compare their number with lower- z SMGs, we use *Herschel* to identify candidate high- z SMGs and strong lensing to provide the signal-to-noise and a unique spatial resolution. This technique has now proven quite successful in the study of high- z SMG (e.g. Smail et al 1997; Pelló et al. 1999; Swinbank et al. 2010;

Lestrade et al. 2010; Negrello et al. 2010; Lupu et al. 2011; Cox et al. 2011).

Strongly lensed sources are quite rare on the sky, and are serendipitously discovered in large surveys, such as the South Pole Telescope survey (Vieira et al. 2010), the *Herschel* HERMES (Oliver et al. 2010), or the huge area *Herschel*-ATLAS (H-ATLAS) survey (Eales et al. 2010). We have undertaken a more targeted survey with *Herschel*, focusing on galaxy clusters. Our key project, "Herschel Lensing Survey" (HLS-deep), has the goal to deeply image 44 massive clusters of galaxies with PACS and SPIRE (Egami et al. 2010; Rex et al. 2010), and continues with a SPIRE snapshot survey (HLS-snapshot) of ~ 300 clusters. The unique aim of the HLS survey is to find cluster-lensed sources, as opposed to galaxy-lensed objects found in field surveys such as H-ATLAS. These cluster-lensed sources suffer less from differential amplification than galaxy-lensed sources, while the dense environment of clusters increases the probability of galaxy lensing (Smail et al 2007).

The HLS-deep survey is now fully executed and the source behind Abell 773 is the strongest source at $500\mu\text{m}$, among the 44 clusters surveyed. Together with the $z = 2.78$ lensed galaxy in the Bullet cluster (Rex et al. 2010), it is one of only two HLS-deep SPIRE sources with a peak flux density at $500\mu\text{m}$ above 100 mJy . It is located far from the cluster center ($\sim 4.5' = 1 \text{ Mpc}$), and likely lensed by a single galaxy.

We present in this letter the continuum and molecular line observations of the Abell 773 SMG, deriving its gas excitation and physical properties. §2 reports the discovery of the SMG from our SPIRE and SMA data, IRAM spectroscopic observa-

Send offprint requests to: F. Combes

tions to derive its redshift, with detections of CO, C I, H₂O, [NII] lines and CO(2-1) with EVLA. In §3 we model the data to infer the dust and gas content and its general properties. For distances we adopted the Λ -CDM concordance model: $H_0 = 71$ km/s/Mpc, $\Omega_M = 0.27$ and $\Omega_\Lambda = 0.73$.

2. Observations

2.1. Herschel and SMA

SPIRE observations were conducted using the "large-map mode", with orthogonal cross-linked scans producing $17' \times 17'$ coverage in each of the three SPIRE bands. The maps include 20 repetitions with a total observing time of 1.7 hours, giving an on-source integration time of ~ 2000 s. The data were reduced using the Herschel interactive pipeline environment (HIPE v5.0). The maps were produced with the standard naive map maker, but include additional turnaround data with scan speeds $> 0.5''/s$ to increase the depth of the outer regions of the maps. For more details see Egami et al. (2010).

HLSJ091828.6+514223 was discovered in the SPIRE map of the $z=0.22$ cluster Abell 773 (Barrena et al. 2007), shown in Figure 1. Its position is $\alpha_{2000} = 09^h 18^m 28.6^s$ and $\delta_{2000} = 51^\circ 42' 23.3''$, too far away to be covered by PACS or *Spitzer* images of the cluster. It lies close to an optical source (Fig 1), which is likely the lensing galaxy. HLSJ091828.6+514223 has an SED (spectral energy distribution) peaking at $500\mu\text{m}$, with $F_{500}=203$ mJy, suggesting a high redshift. The mm/submm contribution of the foreground galaxies is negligible.

The Submillimeter Array (SMA) observed the source at 235 GHz (1.3 mm) on 15 Jun 2011 with precipitable water vapor (pwv) between 1.5 and 4mm during 62min on-source, with 8 GHz total bandwidth. The source was reobserved at 341 GHz ($880\mu\text{m}$) on 9 Dec 2011, during 330 minutes on-source and pwv of 1.5mm. Phase and amplitude gain variations with time were monitored using quasars 0927+390 and 0920+446, and the flux scale was determined using Titan (Table 1). The source is slightly resolved at 1.3mm by the $4.6 \times 2.8''$ beam, and resolved at $880\mu\text{m}$ by the $2.1 \times 2.0''$ beam, with an N/S extension (Fig 1).

2.2. IRAM and EVLA

To measure the redshift of the source, we used the strategy developed by Weiss et al. (2009) and Lestrade et al. (2010) with the multi-band heterodyne receiver EMIR at the IRAM 30-m telescope. At the time of observations (26-27 Sep and 6 Oct 2011), one setup with the 3mm receivers provided 7.43 GHz of instantaneous, dual linear polarization bandwidth. We then covered the 35 GHz, from 80 to 115 GHz, in five setups with some overlaps, integrating about one hour per setup, in wobbler-switching mode. The precipitable water vapor was between 2 and 5mm, and the system temperatures was 90-100K at 3mm and 200K at 1.3mm. We used two backends, the 4MHz filter-banks, and the WILMA autocorrelator, which provides a spectral resolution of 2 MHz. Pointing and focus offsets, determined once every two hours, were more accurate than $3''$. Continuum levels were obtained at 2mm and 1.3mm (and an upper limit at 3mm, cf Fig. 2 and Table 1). At 1.3mm, we detected 40 ± 5 mJy, slightly lower than, but still compatible with the SMA value.

The search revealed a line only at the fourth setup, at 92.3 GHz. The fifth setup gave a second line at 110 GHz, suggesting a redshift, which was then confirmed by tuning the 2mm receiver at 129 GHz, the three detected lines thus being ^{12}CO J=5-4, J=6-5 and J=7-6 transitions, indicating a redshift of 5.2429. Other

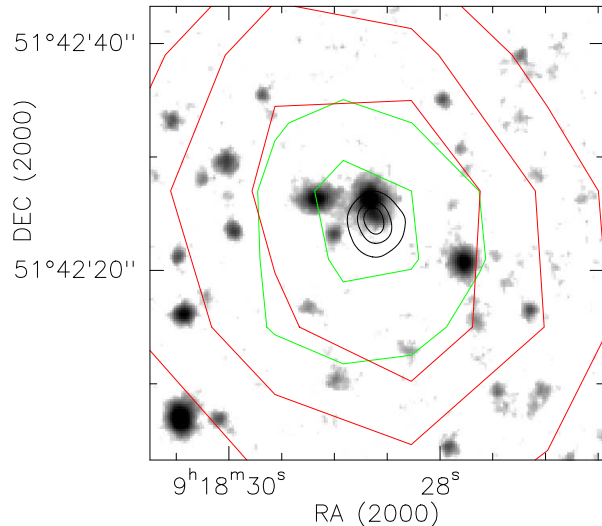


Fig. 1. SPIRE $250\mu\text{m}$ (green, beam $18''$), $500\mu\text{m}$ (red, $37''$) and SMA $880\mu\text{m}$ (black, $2''$) overplotted on the Subaru (suprime cam) V-image of HLSJ091828.6+514223. The latter shows the lensing galaxy at the center, slightly north of the SMA peak. The SMA contours start at 1σ and increase in steps of 4σ . The EVLA CO(2-1) contours are peaked at the same position and have the same N-S elongation.

lines were searched for, such as dense tracers HCN and HCO⁺ at 3mm, water at 2mm, and the [NII] $205\mu\text{m}$ line at 1.3mm.

Around 1 hr of integration was also obtained in CO(2-1) using the Expanded Very Large Array (Perley et al. 2011), with observations and data reduction following those reported by Ivison et al. (2011).

Figure 3 displays all detected lines, and results of the Gaussian fits are reported in Table 2.

3. Results

3.1. Lens modeling

The *V* and *i* images obtained with the Suprime Cam at Subaru shows the presence of a foreground galaxy at $\sim 1.2''$ north of the SMG source. A 3×10 min spectrum was taken on KeckII with DEIMOS 600l/mm grating at 7200\AA with the GG455 filter, centered on the foreground galaxy using a $1''$ slit at PA= 14° in $\sim 1''$ seeing. The spectroscopic redshift of the lens was measured as $z=0.63 \pm 0.005$, from CaII-HK lines and the G band. Adopting an apparent size for the lensed source of $\sim 2''$ from the SMA maps, we have used LENSTOOL (Kneib et al. 1993) to produce Einstein rings or crosses of this size, and estimate a magnification $\mu \sim 11$ (sum of the images) for a lens at $z=0.63$. Since the images are not identified yet, we estimate that 11 is the max-

Table 1. Flux S_ν (mJy) for HLSJ091828.6+514223, with IRAM-30m (I), SMA (S) and *Herschel* (H)

3 mm	2mm	1.3mm	0.88mm	$500\mu\text{m}$	$350\mu\text{m}$	$250\mu\text{m}$
I	I	S	S	H	H	H
<2	15 ± 7	55 ± 7	125 ± 8	203 ± 9	168 ± 8	85 ± 8

Not including absolute flux calibration uncertainties

Table 2. Observed line parameters toward HLSJ091828.6+514223

Line	ν_{obs} [GHz]	T_{mb} [mK]	S_{ν} [mJy]	ΔV_{FWHM} [km s $^{-1}$]	I [Jy km s $^{-1}$]	V^* [km s $^{-1}$]	$L'/10^{10}$ [K km s $^{-1}$ pc 2]	Telescope
CO(2-1) blue	36.9280		3.1 ± 0.7	230 ± 60	0.8 ± 0.1	-530 ± 20	$17. \pm 2.$	EVLA
red			4.0 ± 0.7	510 ± 30	2.2 ± 0.1	-20 ± 20	$55. \pm 3.$	
CO(5-4) blue	92.3077	1.7 ± 0.3	8.6 ± 1.5	110 ± 30	1.0 ± 0.2	-540 ± 12	$4. \pm 1.$	IRAM-30m
red		2.7 ± 0.3	13.4 ± 1.5	540 ± 40	7.7 ± 0.5	-5 ± 17	$30. \pm 2.$	
CO(6-5) blue	110.7615	1.7 ± 0.4	$11. \pm 2$	160 ± 60	1.9 ± 0.4	-540 ± 25	$5. \pm 1.$	IRAM-30m
red		3.1 ± 0.4	$16 \pm 2.$	510 ± 50	8.3 ± 0.6	0 ± 17	$23. \pm 2.$	
CO(7-6) blue	129.2111	2.0 ± 0.3	9.7 ± 1.5	150 ± 20	1.5 ± 0.2	-510 ± 30	$3. \pm .5$	IRAM-30m
red		2.9 ± 0.3	14.3 ± 1.5	560 ± 20	8.5 ± 0.3	4 ± 10	$17. \pm 1.$	and PdBI
C I($^3P_2 - ^3P_1$) blue	129.6422	1.6 ± 0.3	8.3 ± 1.5	150 ± 20	1.4 ± 0.2	-530 ± 9	$2.8 \pm .5$	IRAM-30m
red		1.7 ± 0.3	8.8 ± 1.5	530 ± 40	4.9 ± 0.3	20 ± 14	$10. \pm 1.$	and PdBI
H $_2$ O $_p$ (2,0,2-1,1,1)	158.2481	2.2 ± 0.5	11 ± 2	400 ± 60	4.8 ± 0.7	-17 ± 30	6.5 ± 0.8	IRAM-30m
NII blue	234.0469	1.6 ± 0.2	8 ± 1	410 ± 90	3.5 ± 0.6	-620 ± 35	2.2 ± 0.4	IRAM-30m
red		1.7 ± 0.2	8.7 ± 1	340 ± 60	3.2 ± 0.5	-33 ± 30	2.0 ± 0.4	

Data and errors are derived from Gaussian fits for the two V-components.

* The velocity is given relative to $z=5.2429$ (centered on the red component of the CO(6-5) line)

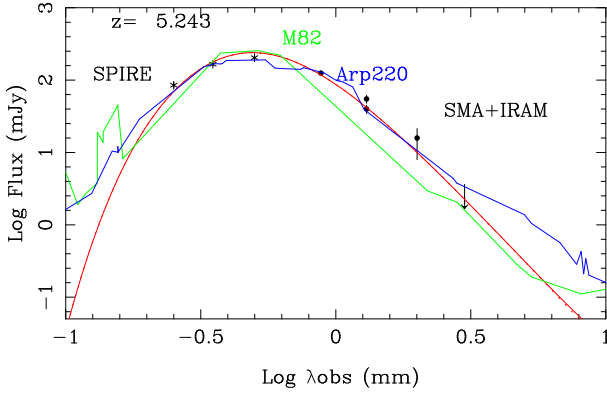


Fig. 2. SPIRE (250, 350 and 500 μm), SMA (0.88 and 1.3mm) and IRAM (1.3, 2 and 3mm) photometric data for HLSJ091828.6+514223, superposed on our model (red line) of a single big grain component at $T_d=52\text{K}$ ($\beta = 2$). The M82 and Arp220 SED from NED are also plotted. Our source has an SED very similar to Arp 220.

imum amplification, whose range is 5-11. The cluster does not boost the magnification by more than 10% (Richard et al. 2010).

3.2. Dust emission

Table 1 displays the available photometric data from SPIRE, SMA and the IRAM-30m. We fitted the data in Fig. 2 with a single optically thin big grain component at an average temperature $T_d=52\text{K}$, an emissivity slope $\beta=2$, and a mass absorption coefficient $\kappa=50 \text{ cm}^2/\text{g}$ at $100\mu\text{m}$. We derived the total FIR(8-1000 μm) luminosity $L_{\text{FIR}} = 1.1 \cdot 10^{14}/\mu L_{\odot}$, and the star-formation rate $\text{SFR} = 1.8 \cdot 10^4/\mu M_{\odot}/\text{yr}$, applying the relation from Kennicutt (1998). Fitting with other dust models, such as Chary & Elbaz (2001), leads to the same luminosity, within the uncertainties. The mass of the dust is then $M_{\text{dust}} = 5.0 \cdot 10^9/\mu M_{\odot}$, which for a gas-to-dust mass ratio of 150 leads to $M_{\text{gas}} = 7.6 \cdot 10^{11}/\mu M_{\odot}$. Other fits are possible, although less good, with lower values of β (down to 1.5), higher dust temperatures and lower dust masses, down by a factor 4.

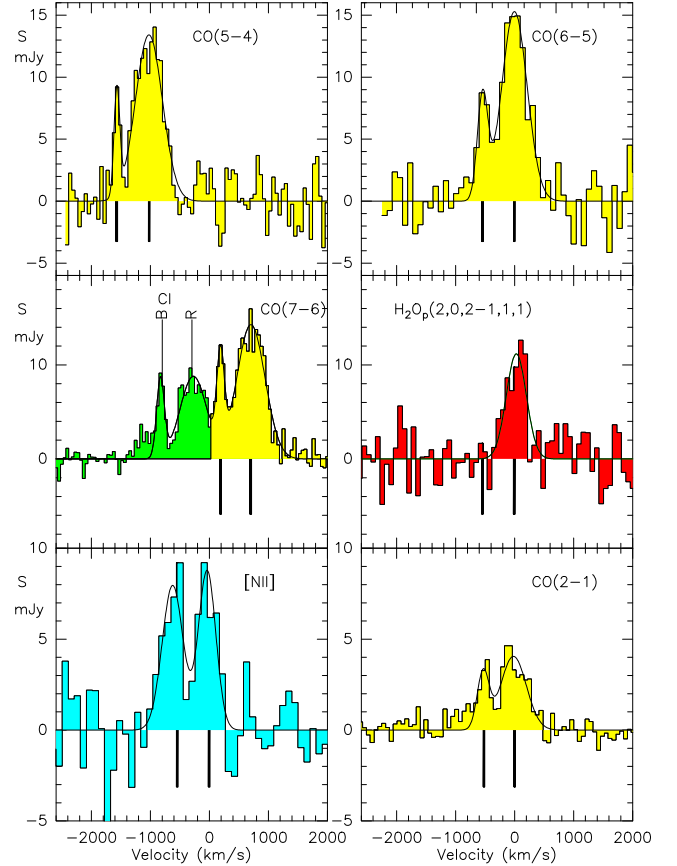


Fig. 3. Four CO lines, with the C I($^3P_2 - ^3P_1$), H $_2$ O $_p$ (2,0,2-1,1,1) and [NII] lines. All spectra are from the IRAM-30m, except for the CI/CO(7-6) from the PdBI, and CO(2-1) from EVLA. Upper vertical lines indicate the red (R) or blue (B) components for CI, and lower vertical lines indicate the same for all others. All panels have the same velocity scale (translated for CO(5-4) and CO/CI). The blue component of the [NII] line is much stronger and broader than for the CO lines, suggesting a strong ionized gas flow. Exact velocities are detailed in Table 2.

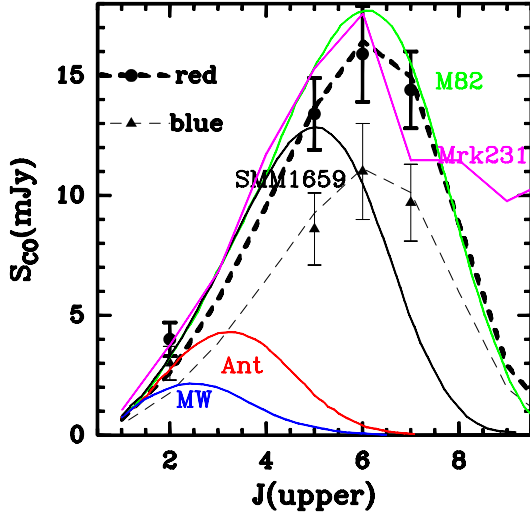


Fig. 4. Peak CO line fluxes for the red (dots) and blue component (triangles), with the best LVG model (bold and light dashed lines, respectively) computed with a density $n_{H_2} = 3.5 \cdot 10^3 \text{ cm}^{-3}$, $T_k = 45\text{K}$, and a column density $N(\text{CO}) = 10^{18} \text{ cm}^{-2}/\text{km s}^{-1}$. The light dashed line is related to the bold line in a ratio of 0.8 to 1. The color lines represent CO data from other galaxies (e.g. Weiss et al. 2007; Danielson et al. 2011).

3.3. CO lines

Four CO lines are clearly detected in two components, as shown in Figure 3. The peak flux of the stronger red component is modeled in Figure 4 with an LVG (large velocity gradient) code, varying the H_2 volume density, the CO column density and the kinetic temperature (Combes et al. 1999). The blue component has a peak intensity lower by 25%, whatever the J level, within the error bars. The three high- J CO lines are well fitted by a single excitation component, peaking at the $J = 6$ level. We found the best fit with a density $n_{H_2} = 3.5 \cdot 10^3 \text{ cm}^{-3}$, $T_k = 45\text{K}$, and a column density $N(\text{CO}) = 10^{18} \text{ cm}^{-2}/\text{km s}^{-1}$. The solution is somewhat degenerate, between low H_2 density and higher CO column density, and we favor optically thick CO emission. PDR (photodissociation region) models fit as well, the CO being emitted by small and dense optically thick clouds. Observations of higher J CO lines are required to distinguish between PDR and XDR (X-ray-dissociated region), where CO is emitted by a more extended and diffuse hot medium (Meijerink et al. 2007). The observed CO(2-1) flux is 50% higher than predicted by the high-excitation component, suggesting the presence of a cooler component, containing one third of the mass. Adopting the conversion factor $M(H_2)/L'_{CO(1-0)} = 0.8 M_\odot / (\text{K km s}^{-1} \text{pc}^2)$ of ULIRGs (ultraluminous galaxies, e.g. Solomon et al. 1997), we derive from the CO(2-1) integrated flux an H_2 mass of $5.8 \cdot 10^{11} / \mu M_\odot$. This mass is 0.8 times that derived from the dust emission, but there are still uncertainties in the conversion ratio to apply. The derived ratio $L_{FIR}/L'_{CO(3-2)} \sim 260$, compatible with other (U)LIRGs (Iono et al. 2009).

3.4. Atomic carbon

Since the $C\text{I}(^3P_1 - ^3P_0)$ line is not available in the receiver range, we have observed the $C\text{I}(^3P_2 - ^3P_1)$ with the 30m, and confirmed it later with the Plateau de Bure (PdBI), with a better signal-to-noise ratio (Boone et al. in prep). The latter is shown in Fig 3, with the two velocity components detailed in Table 2. From

an adopted excitation temperature of $T_{ex} = 40\text{K}$, and a total luminosity $L'_{C\text{I}(^3P_2 - ^3P_1)} = 12.8 \cdot 10^{10} \text{ K km s}^{-1} \text{pc}^2$, we derive a carbon mass of $M_{C\text{I}} = 2 \cdot 10^8 / \mu M_\odot$ (Weiss et al. 2005). This yields a $C\text{I}/H_2$ number abundance of $6 \pm 2 \cdot 10^{-5}$, comparable to other high- z SMGs (e.g. Danielson et al. 2011).

3.5. Water

ISO and *Herschel* observations have revealed that far-infrared H_2O lines are surprisingly strong with respect to CO in ULIRGs, in particular those containing an AGN (Arp 220, Cloverleaf, Mrk 231, Gonzalez-Alfonso et al. 2004, 2008; Bradford et al. 2009; van der Werf et al. 2010). Water is thought to evaporate from grains in shocked regions, in dense hot cores due to cosmic rays or possibly X-rays near AGN (Gonzalez-Alfonso et al. 2010). In Mrk231, van der Werf et al. (2010) have shown that starbursts and PDR alone cannot explain the high- J excitation of the CO lines, nor the H_2O/CO ratios, and a very strong FIR radiation field or XDR conditions related to AGN are required. The associations of starbursts with AGN might be even more frequent at high redshift, and a strong H_2O line has been detected at $z=2.3$ (Omont et al. 2011) and $z=3.91$ (e.g. van der Werf et al. 2011).

The water line detected in HLSJ091828.6+514223 is the highest flux line expected from the mixed model of Gonzalez-Alfonso & Cernicharo (1999), including collisional excitation and far-infrared pumping. We did not detect the $H_2O_o(1,1,0-1,0,1)$, with an upper limit 3 times lower than the $H_2O_p(2,0,2-1,1,1)$ line, which is compatible with the model (expected ratio of 4). The water lines are very optically thick, but information comes from their ratio to the CO lines, which here is $I(H_2O)/I(CO) \sim 0.5$, equal to the ratio observed in Mrk231 or the Cloverleaf quasar at $z=2.6$, SDP.17b at $z=2.3$, and a little lower than in APM08279 at $z=3.91$ (van der Werf et al. 2011, and references therein). In all these galaxies, this ratio is 1-2 orders of magnitude higher than in Orion bar. This suggests the existence of a hot dense component, or an XDR in HLSJ091828.6+514223.

3.6. The $[\text{NII}]205\mu\text{m}$ line

Figure 3 displays the spectrum of the $^3P_1 - ^3P_0$ ground state fine structure line of ionized nitrogen, smoothed to a resolution of 100 km s^{-1} . The two velocity components are clearly detected, and the blue component is much broader than for the CO and CI lines. This fine structure line, with a low excitation potential, mainly traces HII regions photoionized by OB stars. In the Milky Way, the line appears moderate, with an intensity ratio $[\text{CII}]/[\text{NII}] \sim 10$. The latter ratio is 20 in M82 (Petuchowski et al. 1994), and 15 in Mrk231 (Fischer et al. 2010). Only upper limits have been reported in high- z galaxies, the most constraining being in the J1148+5251 quasar at $z=6.4$ (Walter et al. 2009), with $L_{[\text{NII}]} / L_{FIR} < 2 \cdot 10^{-5}$, and $L_{[\text{NII}]} / L_{CO(6-5)} < 0.9$. Here we detect the line with $L_{[\text{NII}]} / L_{FIR} = 4 \cdot 10^{-5}$ and $L_{[\text{NII}]} / L_{CO(6-5)} = 0.15$. These values are intermediate between the AGN-dominated Mrk231, where $L_{[\text{NII}]} / L_{FIR} = 0.8 \cdot 10^{-5}$, and the starburst M82, where $L_{[\text{NII}]} / L_{FIR} = 7.5 \cdot 10^{-5}$. The broad line seen in the $[\text{NII}]$ blue velocity component could be related to galactic winds, often seen in AGN/starburst composite ULIRGs, and with higher velocities than in neutral flows (Veilleux et al. 2005; Rupke et al. 2005; Fischer et al. 2010).

Table 3. Line upper limits at 3σ in channels of 140 km s^{-1}

Line	ν_{obs} (GHz)	S_ν (mJy)*
HCN & HCO ⁺ (6-5)	~ 86 .	< 4 .
¹³ CO(5-4)	88.2484	< 10 .
H ₂ O _v (1,1,0-1,0,1)	89.2111	< 4 .
CS(11-10)	86.2882	< 10 .

3.7. Other lines

We have searched for the high-density tracers HCN and HCO⁺, in their lowest available level, i.e. J=6-5 (Table 3). The upper limits found HCN(6-5)/CO(6-5) < 0.25 are not yet constraining, since ULIRGs have on average HCN/CO ~ 0.1 , except for 1 or 2 luminous quasars (Gao & Solomon 2004).

4. Discussion and conclusion

We have estimated an amplification $\mu \lesssim 11$ from LENSTOOL (likely range 5-11). The amplification factor can also be estimated from the trend of the CO(1-0) *FWHM* line width with luminosity L (Harris et al. 2012; Bothwell et al. 2012 in prep): $\mu = 3.5 * (L'/10^{11} \text{ K km s}^{-1} \text{ pc}^2) * (FWHM/400 \text{ km s}^{-1})^{-1.7}$. This yields $\mu = 16 \pm 5$, which is consistent with our earlier estimate, and suggests that the amplification is likely ~ 11 . Taking into account this magnification, the intrinsic FIR luminosity of the source is still in the $\sim 10^{13} L_\odot$ range, corresponding to a hyper-luminous source. The detected lines (except water) are divided into two velocity components, which suggests a galaxy merger, and would explain the high derived SFR (Engel et al. 2010).

At these high luminosities, an AGN component is probable, which is supported by the high water emission. However, the flux in the CO ladder peaks at $J = 6$ as in starbursts like NGC 253 and M82, and we have no evidence yet that it is extended to higher J as in powerful AGNs like Mrk231 or APM08279. The [NII]205 μm line is detected for the first time at high- z , and its relative luminosity with respect to L_{FIR} is intermediate between a starburst (M82) and an AGN (Mrk231). Its blue velocity component is much broader than for the CO lines, which could come from violent flows of ionized gas. The two velocity components have quite different properties (in H₂O, [NII]), favoring an interpretation in terms of two galaxies, with a high velocity difference of 540 km s^{-1} . Observations of the higher- J CO lines are needed to complete the gas excitation, and interferometer maps of key lines, such as the [CII] line, will bring more information about the nature of this interesting system.

Acknowledgements. IRAM is supported by INSU/CNRS (France), MPG (Germany) and IGN (Spain). Herschel is an ESA space observatory with instruments provided by European-led PI consortia and with important participation from NASA. Support for this work was provided in part by NASA through an award issued by JPL/Caltech. The SMA is a joint project between the Smithsonian Astrophysical Observatory and the Academia Sinica Institute of Astronomy and Astrophysics and is funded by the Smithsonian Institution and the Academia Sinica. NRAO is operated by Associated Universities Inc., under a cooperative agreement with the National Science Foundation. The Keck observatory, made possible thanks to the generous support of W. M. Keck Foundation, is operated by Caltech, the University of California, and NASA.

References

Barrena R., Boschin W., Girardi M., Spolaor M. 2007, A&A 467, 37
Bradford C.M., Aguirre J.E., Aikin R. et al. 2009, ApJ 705, 112
Chary R., Elbaz D. 2001, ApJ 556, 562
Combes F., Maoli R., Omont A. 1999 A&A 345, 369
Cowie, L.L., Songaila, A., Hu, E. M., Cohen, J. G. 1996, AJ 112, 839

Cox P., Krips M., Neri R. et al. 2011, ApJ 740, 63
Danielson A.L.R., Swinbank A.M., Smail I. 2011, MNRAS 410, 1687
Dole, H., Lagache, G., Puget, J.-L. et al. 2006, A&A 451, 417
Eales, S., Dunne, L., Clements, D. et al. 2010, PASP, 122, 499
Egami, E., Rex, M., Rawle, T. D. et al. 2010, A&A 518, L12
Engel H., Tacconi L., Davies R.L. et al. 2010, ApJ 724, 233
Fischer, J., Sturm, E., Gonzalez-Alfonso, E.; et al. 2010, A&A 518, L41
Gao Y., Solomon P.M. 2004, ApJS 152, 63
Genzel R., Baker, A. J., Tacconi, L.J et al. 2003, ApJ 584, 633
Gonzalez-Alfonso, E., Cernicharo J. 1999 ApJ 525, 845
Gonzalez-Alfonso, E., Smith H., Fischer J., Cernicharo J. 2004 ApJ 613, 247
Gonzalez-Alfonso, E., Smith H., Ashby M. et al. 2008 ApJ 675, 303
Gonzalez-Alfonso, E., Fischer J., Isaak K. et al. 2010 A&A 518, L43
Harris A.I. et al. 2012, ApJ sub.
Heavens, A., Panter, B., Jimenez, R., Dunlop, J. 2004, Nature 428, 625
Hickox R.C., Wardlow J.L., Smail I. et al. 2011, MNRAS (arXiv1112.0321)
Iono, D., Wilson, C. D., Yun, M.S. et al. 2009, ApJ, 695, 1537
Ivison R.J., Papadopoulos, P. P., Smail, I. et al. 2011, MNRAS 412, 1913
Kennicutt, R. 1998, ARAA 38, 189
Kneib J-P., Mellier, Y., Fort, B., Mathez, G. 1993 A&A 273, 367
Lacey, C. G., Baugh, C. M., Frenk, C. S. et al. 2010 MNRAS 405, 2
Lestrade J-F., Combes F., Salomé P. et al. 2010 A&A 522, L4
Lupu, R. E., Scott, K. S., Aguirre, J. E. et al. 2011, ApJ, sub (arXiv1009.5983)
Magnelli, B., Elbaz, D., Chary, R. R. et al. 2009 A&A, 496, 57
Magnelli, B., Elbaz, D., Chary, R. R. et al. 2011 A&A, 528, 35
Negrello M., Hopwood, R., De Zotti, G. et al. 2010, Science, 330, 800
Oliver S.J., Wang, L., Smith, A. J. et al. 2010, A&A 518, L21
Omont A., Neri R., Cox P. et al. 2011, A&A 530, L3
Meijerink R., Spaans M., Israel F.P. 2007, A&A 793, 811
Pelló R., Kneib, J. P., Le Borgne, J. F. et al. 1999, A&A 346, 359
Pérez-González P.G., Rieke G.J., Villar V. et al. 2008, ApJ 675, 234
Perley R. A., Chandler, C. J., Butler, B. J., Wrobel, J. M., 2011, ApJ 739, L1
Petuchowski, S. J., Bennett, C. L., Haas, M. R. et al. 1994, ApJ 427, L17
Rex, M., Rawle, T. D., Egami, E. et al. 2010, A&A 518, L13
Richard, J., Smith, G. P., Kneib, J-P. et al. 2010, MNRAS 404, 325
Riechers D., Weiss A., Walter F., Wagg J. 2010, ApJ 725, 1032
Riechers D., Carilli C., Walter F. et al. 2011, ApJ 733, L11
Rupke, D.S., Veilleux, S., Sanders, D.B. 2005, ApJ 632, 751
Smail, I., Ivison, R. J., Blain, A. W. 1997, ApJ, 490, L5
Smail, I., Swinbank, A. M., Richard, J. et al. 2007, ApJ 654, L33
Solomon P.M., Downes D., Radford S. J. E., Barrett, J. W. 1997, ApJ 478, 144
Swinbank A.M., Chapman, S. C., Smail, I. et al. 2006, MNRAS 371, 465
Swinbank A.M., Smail, I., Longmore, S. et al. 2010, Nature, 464, 733
van der Werf P., Isaak K., Meijerink R. et al. 2010, A&A 518, L42
van der Werf P., Berciano Alba A., Spaans M. et al. 2011, ApJ 741, L38
Veilleux, S., Cecil, G., Bland-Hawthorn, J. 2005, ARAA 43, 769
Vieira J.D., Crawford T.M., Switzer E.R. et al. 2010, ApJ 719, 763
Walter F., Weiss A., Riechers D. et al. 2009, ApJ 691, L1
Wardlow, J. L., Smail, I., Coppin, K.E.K. et al. 2011, MNRAS 415, 1479
Weiss A., Downes D., Henkel, C., Walter F. 2005, A&A, 429, L25
Weiss A., Downes D., Neri R., et al. 2007, A&A 467, 955
Weiss A., Ivison R.J., Downes D. et al. 2009, ApJ, 705, L45

-
- ¹ Observatoire de Paris, LERMA, CNRS, 61 Av. de l'Observatoire, 75014 Paris, France e-mail: francoise.combes@obspm.fr
 - ² Steward Observatory, University of Arizona, 933 North Cherry Avenue, Tucson, AZ, 85721, USA
 - ³ Université de Toulouse, UPS-OMP, CNRS, IRAP, 9 Av. colonel Roche, BP 44346, 31028, Toulouse Cedex 4, France
 - ⁴ Institute for Computational Cosmology, Durham University, South Road, Durham, DH1 3LE, UK
 - ⁵ CRAL, Université Lyon-1, 9 Av. Charles André, 69561 St Genis Laval, France
 - ⁶ UK Astronomy Technology Centre, Royal Observatory, Blackford Hill, Edinburgh, EH9 3HJ, UK
 - ⁷ Harvard-Smithsonian Center for Astrophysics, 60 Garden Street, Cambridge, MA 02138, USA
 - ⁸ Institute for Astronomy, University of Hawaii, 2680 Woodlawn Dr, Honolulu, HI 96822, USA
 - ⁹ Institut d'Astrophysique de Paris, UPMC and CNRS, 98 bis Bd. Arago, 75014 Paris, France
 - ¹⁰ ASTRON, P.O. Box 2, NL-2990 AA Dwingeloo, The Netherlands
 - ¹¹ Geneva Observatory, Université de Genève, 51 chemin des Maillettes, 1290, Versoix, Switzerland
 - ¹² LAM, CNRS- Université Aix-Marseille, 38 rue F. Joliot-Curie, 13388, Marseille Cedex 13, France
 - ¹³ Academia Sinica Institute of Astronomy and Astrophysics (ASIAA), P.O. Box 23-141, Taipei 10617, Taiwan
 - ¹⁴ Dep. de Astrofísica, Facultad de CC. Físicas, Universidad Complutense de Madrid, 28040 Madrid, Spain
 - ¹⁵ School of Physics and Astronomy, University of Birmingham, Edgbaston, Birmingham B15 2TT, UK
 - ¹⁶ Leiden Observatory, Leiden University, PO Box 9513, 2300 RA, Leiden, The Netherlands